

# SOLAR - STELLAR ATMOSPHERIC TOMOGRAPHY WITH MM-RADIO SNAPSHOT SPECTROSCOPIC IMAGING

A. Mohan<sup>1,2</sup>

## Abstract

Millimeter (mm) frequencies are primarily sensitive to thermal emission from layers across the stellar chromosphere up to the transition region, while metre-wave (radio) frequencies probe the coronal heights. Together the mm and radio band spectroscopic snapshot imaging enables the tomographic exploration of the active atmospheric layers of the cool main-sequence stars (spectral type: FGKM), including our Sun. Sensitive modern mm and radio interferometers let us explore solar/stellar activity covering a range of energy scales at sub-second and sub-MHz resolution over wide operational bandwidths. The superior uv-coverage of these instruments facilitate high dynamic range imaging, letting us explore the morphological evolution of even energetically weak events on the Sun at fine spectro-temporal cadence. This article will introduce the current advancements, the data analysis challenges and available tools. The impact of these tools and novel data in field of solar/stellar research will be summarised with future prospects.

## 1 Introduction

Solar and stellar activity refers to a range of phenomena happening across the atmospheres of the sun/other cool main sequence stars (spectral type F - M), which lead to observable variability in their typical background/quiescent emission. These phenomena are driven by a variety of physical processes occurring across various outer atmospheric layers of the star starting from photosphere to corona (see, Magara et al., 1997; Cliver et al., 2022, for an overview) Such active phenomena vary over a wide range of spatial, temporal and energy ranges. Their spatial scales vary within  $\sim 100 - 10^5$  km, (e.g. Yashiro et al., 2004; Shibata et al., 2007; Namekata et al., 2022), time scales from a few ms to hours(e.g. Osten et al., 2008; Aschwanden & Freeland, 2012; Saint-Hilaire et al., 2013; Villadsen & Hallinan, 2019; Dal, 2020) and energy scales within  $\sim 10^{23} - 10^{36}$  erg (e.g. Aschwanden &

---

<sup>1</sup>Roseland Centre for Solar Physics, University of Oslo, Postboks 1029 Blindern, N-0315 Oslo, Norway

<sup>2</sup>Institute of Theoretical Astrophysics, University of Oslo, Postboks 1029 Blindern, N-0315 Oslo, Norway

Freeland, 2012; Namekata et al., 2017). Several of these phenomena finally impact the space-weather via large scale outflows and high energy particle activity, which can have huge impacts on the atmospheres of close-in planets (e.g. Segura et al., 2010; Vidotto et al., 2013). This makes the study of active phenomena on the sun (and stars) important from the perspective of their Earth/ionospheric-impact (and exo-planet habitability). In order to explore the cross atmospheric evolution of these phenomena, given their variability scales, we need a high cadence ( $\lesssim 1$  s) tomographic observing technique sensitive to the different heights across the active stellar atmospheric layers, namely chromosphere and corona. It is within these active layers that different non-equilibrium processes dump a lot of excess magnetic field free energy to the local plasma resulting in frequent heating and particle acceleration over a range of energies (e.g. Linsky, 2017; Aschwanden & Freeland, 2012).

### 1.1 Tomographic exploration of active atmospheric layers

Active atmospheric layers radiate energy across the entire electromagnetic spectrum, during both flaring and non-flaring periods. The UV to soft X-ray continuum primarily tracks the coronal thermal emission from hot plasma, while the hard X-ray spectrum gives the information about accelerated particles. These accelerated particles are expected to stream both upwards into interplanetary space generating radio bursts and downwards across chromospheric layers generating various spectral line emission signatures and finally photospheric white light flares (Namekata et al., 2017). Meanwhile, millimeter emission tracks chromospheric heating signatures. See, Fig. 1 for an overview of the various emission sites during a typical solar flare.

The Xray band though sensitive to corona, the emission can span a range of coronal heights since the waveband is optically thin. So, the Xray observations generally provide a line of sight averaged thermal and non-thermal evolution. However, in the case of the Sun, where spatially resolved imaging observations are possible, imaging of off disk-centre sources can be used to gain a sense for emission heights (Masuda et al., 1994). But, this technique cannot be applied to stellar observations where sources are unresolved. However, spectral line inversions can be done using simultaneous multi-line data to infer formation heights across chromosphere to corona. But, they suffer from various non-LTE and propagation effects introducing degeneracy in the emission contribution function and the local physical mechanisms making it difficult to accurately infer emission heights (e.g. Mashonkina et al., 2017; Jeffrey et al., 2017; Kontar et al., 2017b; Zhou et al., 2022). Also, the time resolution obtained in multi-line spectral inversion studies is of the order of  $\sim 10$  s to min even for stellar flares, making it difficult to trace seconds scale non-equilibrium dynamics, known to exist from high cadence radio/mm, UV and Xray observations (e.g. Dennis, 1985; Osten et al., 2008; Endo et al., 2010; Saint-Hilaire et al., 2013).

Meanwhile, meterwave radio bursts primarily originate as coherent emission across coronal heights, at the local plasma frequency ( $\nu_p$ ) and(or) its harmonic. Since local  $\nu_p$  is a function of local density ( $n_e$ ) in the corona, the emission heights can be inferred using a typical density model (e.g. Reid & Ratcliffe, 2014; Zucca et al., 2014). This property lets us explore the propagation of high energy particles and active phenomena across coronal

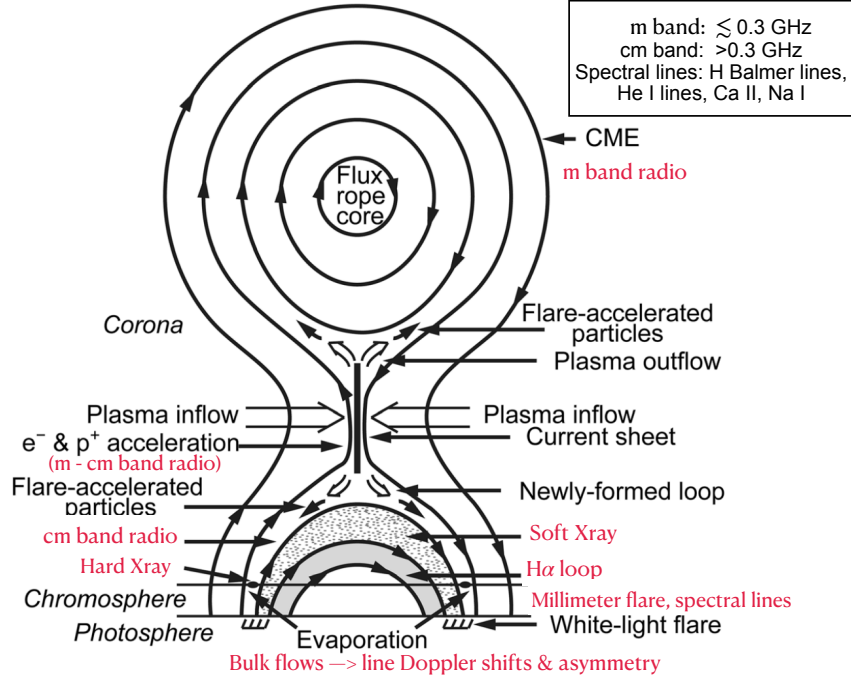


Figure 1: Standard flare model showing a flaring active region loop. The magnetic reconnection site is shown with the current sheet and bi-directional accelerated particle beams marked. The different emission regions across all atmospheric layers are also shown (see, text for details). Important spectral lines are mentioned in the box. Evaporation and downflows produce spectral Doppler shifts and asymmetric line profiles. (Figure credit: Cliver et al., 2022).

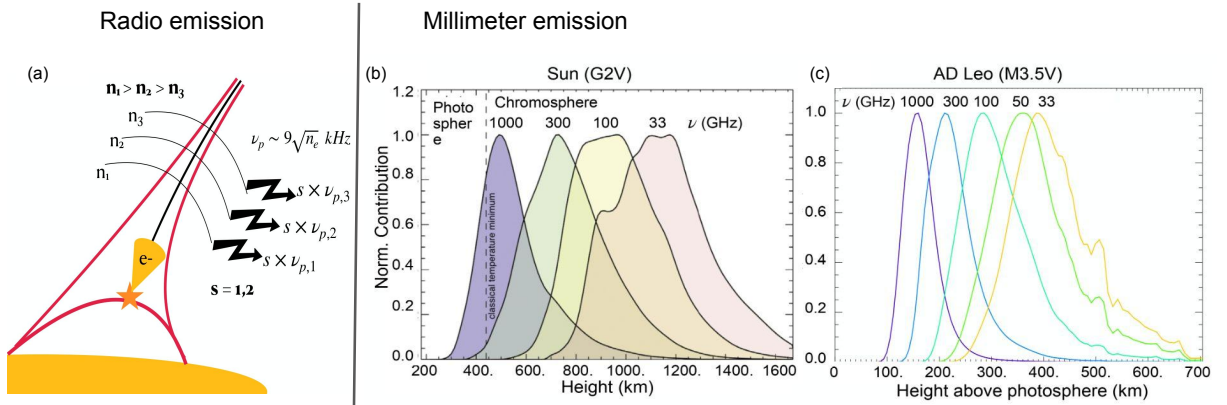


Figure 2: Graphical summary of the idea of tomographic imaging. (a) Metrewave frequencies arising from varying atmospheric heights as the accelerated electron beams trigger instability across iso-density layers. (b) Millimeter emission contribution functions computed for the different ALMA bands using radiative transfer simulations applied on 3D atmospheric models. Plot for the sun is adapted from (Wedemeyer et al., 2016).

heights (e.g. Morosan et al., 2014; Zucca et al., 2014; McCauley et al., 2018). Figure 2(a) graphically depict the idea of coronal tomography with radio imaging spectroscopy. Similarly, emission at different mm frequencies form at LTE across chromospheric heights in sun-like stars with different frequencies having different penetration depths, acting as a linear thermometer (Wedemeyer et al., 2016). Figure 2(b-c) presents the mm band contribution function models for the Sun and AD Leo (M4V). However, in the case of

strong M-dwarf flares from highly magnetised environments mm-continuum may track gyro-synchrotron emission. This can clearly be separated from the thermal contribution based on emission spectral index and polarisation evolution during the event, offering a unique means to get estimates for local magnetic fields and accelerated particle spectrum alongside thermal evolution across chromospheric layers (e.g. MacGregor et al., 2018). Thus simultaneous mm and radio observations can provide a tomographic view of the dynamics and propagation of various active phenomena like flare, eruptions etc. across the active solar/stellar atmospheric layers from chromosphere to corona. Together with the high energy (Xray to optical) imaging spectroscopy, which provide complementary information on thermal and non-thermal plasma evolution across atmospheric layers, we can better constrain the models and infer local physics (e.g. Osten et al., 2005; MacGregor et al., 2018; Zic et al., 2020). Besides the active emission, quiescent mm emission helps probe the solar/stellar atmospheric heating gradient which is an important input to stellar atmospheric models (e.g. Trigilio et al., 2018; White et al., 2020; Mohan et al., 2021).

**Solar-stellar connection:** Sun being the only spatially resolvable main sequence star, is a an excellent example to study the various types of radio/mm bursts (in time-frequency plane), their physical manifestations and space weather impacts using detailed image plane analysis. There has been several studies of solar flare and quiescent emission in radio and mm bands done in coordination with multi-waveband observations and modelling (see, McLean & Labrum, 1985; White, 2007; Wedemeyer et al., 2016, for an overview). These studies have provided valuable insights on the physics of various active phenomena and their multi-waveband observables. However, it is not necessarily right to directly extend the inferences from the numerous solar activity studies to stars. For instance there has been no sign of type-II radio burst yet detected in the most active M-dwarf stars despite several long term monitoring campaigns (e.g. Villadsen & Hallinan, 2019). The number of CMEs itself is found to lower in active M dwarfs than what is expected from simply extending the solar paradigm (e.g. Leitzinger et al., 2014; Odert et al., 2020). A prominent belief is that, this is possibly due to the strong magnetic field strengths in M-dwarf coronae which results in high Alfvén speeds, that in turn block most flares from causing eruptions. In case of erupting prominences, the high Alfvén speeds could be stopping the shock formation and in turn causing the lack of type-II radio bursts which are associated with CME shocks(e.g. Mullan & Paudel, 2019; Odert et al., 2020). Even young G dwarfs like EK Dra is known to deviate from standard solar flare picture atleast during superflares. Hours-long lasting white light flare with an extent similar to chromospheric  $H\alpha$  flare has been reported in EK Dra (Namekata et al., 2017). In solar flares, usually white light flares last for about half the duration of  $H\alpha$  flares. This anomalously long lived white light flaring in EK Dra is thought to be due to a possible radiative back-warming of photosphere from flare heated chromospheric plasma. Besides, in the case of coherent metrewave ( $\sim 100$  MHz) bursts, young active M dwarfs stars are known to produce highly polarised metric band flares often akin to Electron Cyclotron Maser emission (ECME), besides the coherent plasma emission mechanism (see, Vedantham, 2021, for an overview). Around  $\sim 100$  MHz, ECME mechanism is not that common in the sun given the magnetic field strengths and densities in the corona (Gary, 2001). So while extending the solar

paradigm, one should ensure that the stars are similar atleast in the sense of activity characteristics to the sun. The F to early M type stars with mass greater than  $\sim 0.35 M_{\odot}$  have an inner radiative and outer convective zone like the sun (Chabrier & Baraffe, 2000). Besides, the stellar activity is known to evolve with age (e.g. Skumanich, 1972; Donati & Landstreet, 2009; Vidotto et al., 2014). Barnes (2003) showed that the stars older than 1 Gyr typically falls in the low activity branch, usually referred to as ‘I’. So the insights gained from solar observations could be extended to atleast sun-like stars belonging to F- early M spectral type and ages  $\gtrsim 1$  Gyr. However, the plasma physics and emission mechanisms generally apply to all stars including the sun. So one needs to interpret the multi-waveband observations after incorporating the right local physical conditions like magnetic field strengths and atmospheric physical structure for the star of interest (see, Güdel, 2002; White, 2004, for an overview).

With the advent of modern interferometric arrays like the MWA, LOFAR, uGMRT, MeerKAT, ALMA, NOEMA etc., sensitive high fidelity spectroscopic imaging observations (spectral resolution:  $\sim 10$  kHz in radio;  $\sim 2$  GHz (continuum) and 0.01 - 10 MHz (spectral line) in mm band<sup>1</sup>) are now possible for the sun and nearby stars at  $\lesssim 1$  s resolution. These facilities together cover  $\sim 10$  MHz - 1 THz wide band in a nearly seamless manner, enabling atmospheric tomography across chromosphere to outer corona (heliocentric height  $\sim 2 R_{\odot}$ ) at high sensitivity (e.g. White, 2004; Morosan et al., 2014; Wedemeyer et al., 2016; Vedantham, 2020; Mohan et al., 2021) However, as always massive advancements comes with new challenges. In this case, it is in the form of big data handling, reduction, analysis, automation and storage.

## 2 Big data problem with modern radio/mm interferometers

The high sensitivity and imaging fidelity of the modern instruments primarily owe to their compact large-N (N: antenna count) architecture, which enables dense u-v coverage. The high spectro-temporal sampling across a large-N array leads to high data rates exceeding  $\sim 1$  TB/h. After analysis the data can expand further. Hence, automated calibration and imaging pipelines (e.g. Mohan & Oberoi, 2017; Mondal et al., 2019) have been and are being built for modern telescopes alongside efficient flagging routines (e.g. Offringa, 2010; Zhang et al., 2023). The final products of the calibration/imaging pipelines are usually calibrated measurement sets (MS) or 4-D image data cubes across time, frequency and angular sky-coordinates (Mohan & Oberoi, 2017). I will present two powerful tools which have been developed to analyse these final products and derive the flux evolution of the sources of interest in the image/visibility plane across fine spectro-temporal scales.

### 2.1 SPatially REsolved Dynamic Spectrum (SPREDS)

SPREDS is a tool intended to operate on calibrated 4D image data cubes of the Sun across spectro-temporal axes (see, Mohan & Oberoi, 2017; Mohan, 2021a). SPREDS is a python code which can operate on across snapshot spectroscopic images parallelly and extract flux

---

<sup>1</sup><https://almascience.eso.org/about-alma/alma-basics>

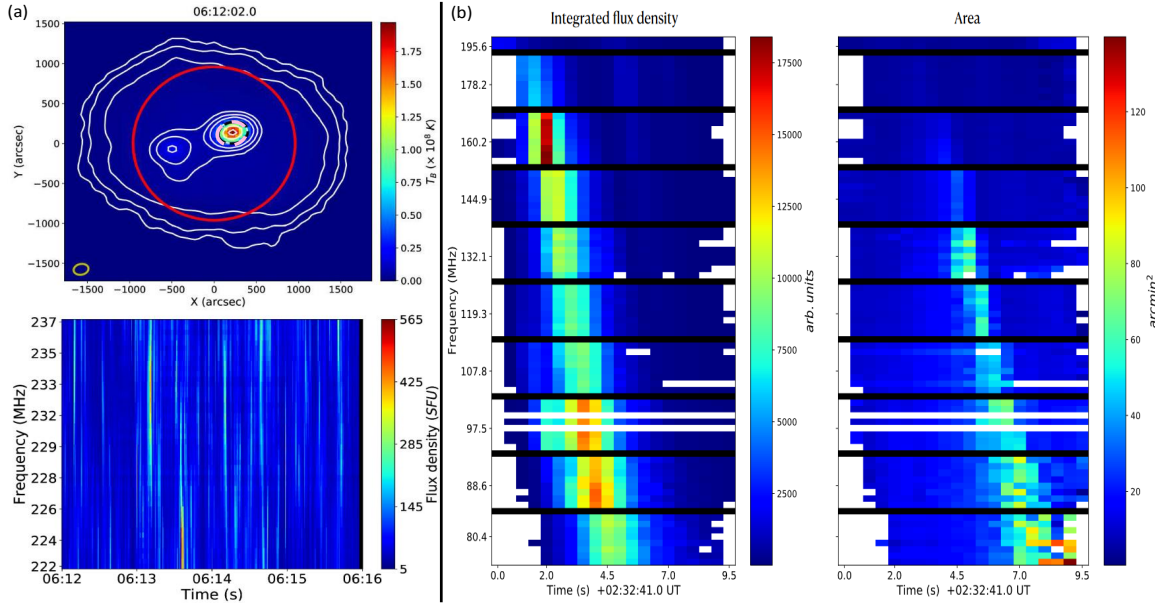


Figure 3: (a) Top: A sample snapshot spectroscopic image made at 0.5 s and 160 kHz resolution using an MWA dataset from 2014-11-03 (Mohan et al., 2019b). Red ring marks the optical solar disk and the pink dotted ellipse marks the chosen  $2\times$  psf region for deriving SPREDS shown in the Bottom panel. (b): SPREDS derived by fitting 2D Gaussian functions to a type-III burst source in a different dataset (Mohan, 2021b).

density from regions of interest on the solar surface. The routine either records the source flux in a user-specified region of any geometric shape or attempts to fit a 2D Gaussian function to the morphology in the specified region to extract the evolution of the size, flux density and orientation of the source. In cases where there is a bright source moving within some region in the image plane, the code can be customised to follow the source and fit 2D Gaussian functions to it.

Figure 3(a) shows an example SPREDS for an elliptical fixed region of the size twice the synthesised beam. The snapshot spectroscopic image (resolution: 0.5 s ; 160 kHz) in the top panel shows the chosen fixed region in black dotted line. Red circle in the image marks the solar disk as seen in visible light data and the synthesised beam (psf) is shown in the bottom left corner of the image. Meanwhile, Figure 3(b) shows the SPREDS derived by fitting 2D Gaussian functions to another burst source close to disk centre, from a different dataset. The resultant SPREDS based on the fitting procedure shows the spectro-temporal evolution of both source area (reported as the elliptical cross sectional area of the best-fit 2D-Gaussian function) and its integrated flux density. A working version of the code is made public via Github<sup>2</sup>, though with less documentation. A more user friendly version with detailed explanation will be released soon.

## 2.2 VISibility Averaged Dynamic spectrum (VISAD)

Unlike solar observations, observations of the cool main-sequence stars do not resolve the star. So imaging is not strictly necessary to explore spectro-temporal evolution of

<sup>2</sup><https://github.com/atul3790/SPREDS>

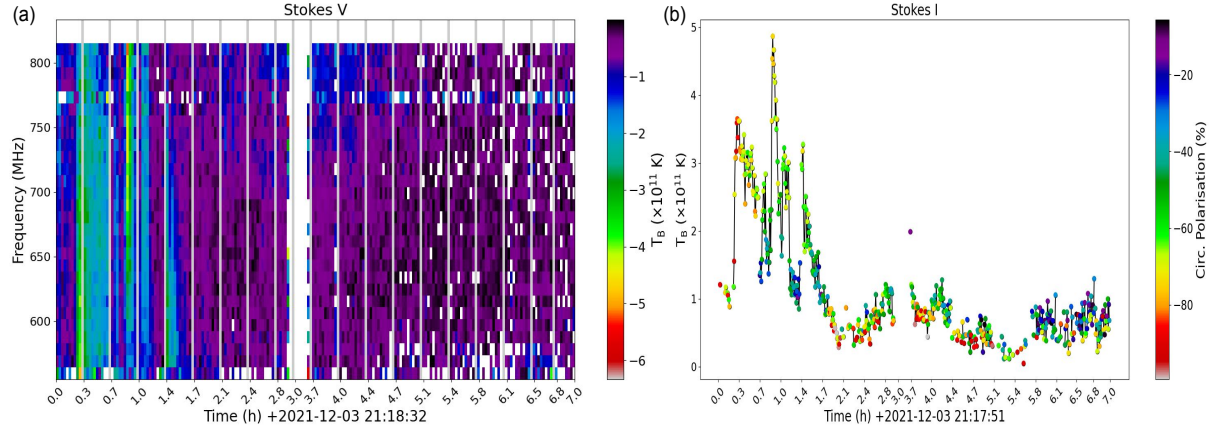


Figure 4: (a): STOKES V VISAD for AD Leo (M4V) at 50s and 5 MHz resolution. (b) Band averaged STOKES I lightcurve with circular polarisation % marked (Mohan et al., in prep).

stellar activity. However, a time averaged imaging of the stellar field is mandatory to obtain a model for the background sky across spectral channels. This background model visibilities can then be subtracted from the corrected data to end up with purely stellar visibility data. VISibility Averaged Dynamic spectrum (VISAD) routine works on this purely stellar spectro-temporal visibility data. VISAD centres the visibility data to the expected location of the star and computes the mean visibility as a function of frequency and time. The routine lets the user choose the required frequency and time averaging so as to detect stellar emission in the dynamic spectral plane. VISAD can generate dynamic spectrum in all STOKES parameters and polarisation supported by the data. It can also generate band averaged light curves. Figure 4 shows STOKES V dynamic spectrum and band-averaged circular polarisation lightcurve for an active M-dwarf AD Leo, made with VISAD applied on uGMRT data (Mohan et al., in prep). The code is equipped with parallel processing capabilities and uses some of the functionalities of Common Astronomy Software Applications (CASA; McMullin et al., 2007) A version of this routine has already been released via Github<sup>3</sup>

The following sections will present some of the key science cases explored using the high resolution snapshot spectroscopic data, applying tools like SPREDS and VISAD.

### 3 Solar activity

Sensitive modern interferometers let us explore the ubiquitous weak radio bursts across all four axes of variability (time, frequency ( $\approx$  height), angular sky coordinates) at much finer resolution than previously possible (e.g. Oberoi et al., 2011; Mohan & Oberoi, 2017; Kontar et al., 2017a). Tools like SPREDS has been a used to study the dynamics of accelerated particles, propagation of waves, instabilities and turbulence across corona at active and quiet solar regions (Oberoi et al., 2022). Some of the interesting discoveries and research avenues that the modern data and tools have opened up are the following.

<sup>3</sup><https://github.com/atul3790/Visibility-averaged-DS>

**Solar flares:** Solar flares often generate a variety of radio and mm bursts. The solar radio bursts, especially the strong ones, have been studied over decades and classified into different burst types (see, Wild, 1970; McLean & Labrum, 1985; White, 2007, for an overview). With the advent of modern sensitive interferometers and spectrographs we are now able to detect weak events, with energy ranges similar to and weaker than microflares (e.g. Ramesh et al., 2013; Suresh et al., 2017; Sharma et al., 2018; Mondal, 2021). Besides, the high spectro-temporal cadence of these instruments also let us probe the fine structures and fast quasi-periodic variability in the emission (e.g. Mugundhan et al., 2017; Kontar et al., 2017a; Sharykin et al., 2018; Mohan et al., 2019a; Mohan, 2021a). Some aspects of these new discoveries pertaining to weak radio bursts will be covered in the paragraphs below.

**3-D Quasi-periodic pulsations (QPP):** Weak radio bursts often trigger quasi-periodic pulsations (QPPs) in the ambient physical fields observable in the image plane. Earlier radio studies had identified such fast  $\sim$ s timescale QPPs during radio bursts in the full disk integrated flux dynamic spectra. However, the evolution of these QPP sources, their spatial distribution and structure remained unexplored until recently, due to limitations in high fidelity spectroscopic snapshot imaging. Recent snapshot spectroscopic imaging studies of the radio counterparts of microflare sources, using SPREDS, revealed that the intensity QPPs are often associated with correlated QPPs in source sizes and sky orientation (Mohan et al., 2019a; Mohan et al., 2019b) giving them a three dimensionality (size, orientation and flux density). Mohan (2021c) showed that these 3-D QPPs had 2 different modes of variability - ‘S’ (size -flux density anti-correlated evolution) and ‘T’ (size - orientation correlated evolution). These modes systematically evolved in tandem with the thermal energy and the local magnetic structure during the microflare. This result reveal a novel means to use QPP diagnostics to explore the local magnetic field evolution at weakly flaring regions, which are otherwise difficult to probe.

**Coronal turbulence and waves:** At coronal heights beyond  $\sim 4R_{\odot}$  and into the solar wind regime, interplanetary scintillation techniques had been used along side other radar-based techniques to infer the density turbulence (Coles et al., 1991; Manoharan & Ananthakrishnan, 1990; Anantharamaiah et al., 1994; Sasikumar Raja et al., 2017). However, in the inner corona we lacked a robust means to characterise the local turbulence. Since coherent radio emission originate at frequencies close to  $\nu_p$ , which is related to local  $n_e$ , wave propagation is heavily influenced by the strength of local density fluctuations ( $\delta n_e/n_e$ ) (see, Steinberg et al., 1971; Robinson, 1983; Thejappa & MacDowall, 1998; Arzner & Magun, 1999; Kontar et al., 2019). This causes rapid ( $\sim$ s) size and shape variability in the observed burst sources alongside observed intensity. Wideband snapshot spectroscopic images lets us explore this variability across inner coronal heights, using techniques like SPREDS (Kontar et al., 2017a; Mohan et al., 2019a). Employing the physical model proposed by Arzner & Magun (1999), Mohan et al. (2019a) derived  $\delta n_e/n_e$  across inner coronal heights (1.4 - 1.45  $R_{\odot}$ ) using MWA data. Later (Mohan, 2021b) extended the study to bursts observed across the entire MWA operational bandwidth (80 - 240 MHz) and estimated the turbulence characteristics of solar corona within  $\sim 1.4 - 1.8 R_{\odot}$ . Similarly by modelling the observed radio wave scattering effects at frequencies



below 80 MHz, turbulence characteristics have been explored up to  $\sim 2.2 R_{\odot}$  by several authors (e.g. Mugundhan et al., 2017; Sharykin et al., 2018; Chen et al., 2020).

Radiowave propagation across corona is also influenced by local plasma wave modes. These effects can be used to infer the spatial scales of the disturbances and properties of their progenitors. For instance, type-III striae bursts offer a means to explore propagating Langmuir waves (e.g. Thejappa & Macdowall, 2018; Reid & Kontar, 2021).

**Radio - CMEs:** CMEs are the most violent eruptions happening on the Sun which leave significant impacts on space weather. However, the particle acceleration sites and their evolution during CMEs remain less understood. High cadence spectro-polarimetric imaging studies have started revealing interesting details on this aspect (see, Carley et al., 2020; Chen et al., 2023, for an overview). CMEs often produce the type-II radio bursts which are believed to be associated with particle acceleration sites around CME shocks (Nelson & Melrose, 1985). The high time resolution radio imaging explorations of these sources using instruments like LOFAR help explore the dynamical evolution of particle acceleration sites across CME shock fronts (e.g. Morosan et al., 2019). Combined with high energy data from multiple spacecrafts at different vantage points, a 3D reconstruction of the evolution of the CME shock and the associated particle acceleration regions can be done (e.g. Zucca et al., 2018; Morosan et al., 2022).

Apart from exploring particle acceleration sites, radio observations of split-band type-II bursts offer a means to compute the Mach number of CME shocks. Combined with white light observations they can help estimate the mean magnetic field strength at the shock regions (Kumari et al., 2017a; Mahrous et al., 2018). Polarimetric studies (degree of circular polarisation) of CME associated radio bursts can also provide estimates of the mean magnetic field strengths at CME shocks (e.g. Sasikumar Raja et al., 2014; Kumari et al., 2017b; Ramesh & Kathiravan, 2022). However, a more direct spatially resolved magnetic field estimation at regions associated with the CME can be performed using imaging observations and subsequent modeling of the gyro-synchrotron emission from various regions in the image plane (e.g. Bastian et al., 2001; Maia et al., 2007; Bain et al., 2014). Such studies however remained difficult due to lower sensitivity of previous generation instruments. Sensitive new generation instruments like MWA are now able to image CME shock fronts that produce order of magnitude weaker radio flux than previous detections (Mondal et al., 2020; Kansabanik et al., 2023a). Modelling the polarised gyro-synchrotron radio spectra from CMEs, the local magnetic field estimates have also been made (Kansabanik et al., 2023a).

**Quiet sun:** Quiet Sun, unlike the name suggest, is expected to be teeming with weaker energy release events which collectively dump enough energy to maintain its high background temperature (see, Parker, 1963; Klimchuk, 2006, 2015, for an overview). Several X-ray to radio band studies have shown evidence for high emission variability at quiet regions or during relatively quiet periods of solar activity (e.g. Mercier & Trottet, 1997; Pauluhn & Solanki, 2007; Testa et al., 2013, 2014; Viall & Klimchuk, 2017). High dynamic range snapshot spectroscopy imaging facilities have enabled the exploration of emission

variability across regions of interest on the quiet sun disk. For instance, studies using high sensitivity MWA data have revealed ubiquitous non-thermal activity down to  $\sim 0.2$  SFU, approaching sub-picoflare energy levels for the first time (e.g. Suresh et al., 2017; Sharma et al., 2018). These are about an order of magnitude weaker than previously reported weakest flaring event (Ramesh et al., 2013). With high resolution snapshot spectroscopic imaging, certain authors have also explored such weak flares across the solar disk and demonstrated its ubiquitous nature (Mondal, 2021; Sharma et al., 2022). Besides, data from MWA and LOFAR have also helped explore the radiowave scattering/propagation effects across quiescent solar disk (Rahman et al., 2019; Sharma & Oberoi, 2020; Zhang et al., 2022). Recent advancements in imaging polarimetry have lead to direct detection of quiet sun magnetic field strengths, which are otherwise impossible to obtain at  $1.1 - 2R_{\odot}$  heights in the corona (McCauley et al., 2019; Kansabanik et al., 2023b). All these observational aspects are crucial in improving the existing solar coronal emission models like FORWARD and making more reliable estimates of the true source energy levels, spatial distribution and morphology (Gibson et al., 2016; Sharma & Oberoi, 2020).

### 3.1 Chromospheric tomography with ALMA

ALMA opened up a new era of solar chromospheric exploration with its high sensitivity and angular resolution at sub-arcsecond scale (depending on the chosen array configuration and frequency). ALMA can provide both total power (TP) brightness temperature maps of the solar disk at  $\sim 8$  s cadence (White et al., 2017a) and also zoomed in interferometric images of selected portions on the solar disk at  $\sim 2$  s resolution (see, Henriques et al., 2022, for an overview on data and results). The TP maps provide an overall idea of the mm emission characteristics across the disk and a means to study the disk averaged sun-as-a-star spectral evolution (Mohan et al., 2022). Meanwhile, the zoomed in multi-band interferometric imaging datasets at high spatio-temporal resolution let us explore propagating waves, shocks and varying chromospheric structure across height (e.g. Wedemeyer et al., 2016; Eklund et al., 2021; Jafarzadeh et al., 2021; Nindos et al., 2022; Narang et al., 2022). Besides, Guevara Gómez et al. (2021) reported structural QPPs akin to the metric 3-D QPPs in high resolution ALMA Band 3 (100 GHz) movies.

## 4 Stellar activity

Sensitive spectroscopic snapshot imaging capability has lead to significant advancements in the field of stellar activity. The advancement is two fold; one in the form of extending the source ‘detectability’ horizon out to distances as high as  $\sim 300$  pc (Vedantham, 2020; Callingham et al., 2021; Vedantham et al., 2022; Callingham et al., 2022), while the other in detecting fine scale spectro-temporal variability (Osten et al., 2008; Crosley & Osten, 2018). These studies have already questioned our understandings about radio flare flux levels, and their relation with other waveband fluxes and physical properties (e.g. Vedantham, 2021; Vedantham et al., 2022). New instruments have also lead to discoveries of star-planet interaction signatures (Vedantham et al., 2020). Tools like VISAD

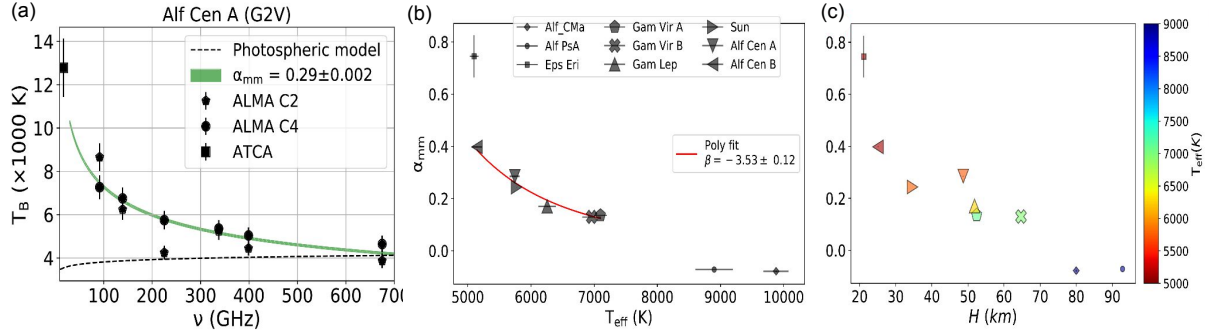


Figure 5: (a):  $mm$ - $T_B(\nu)$  for  $\alpha$  Cen A. Dotted line shows the photospheric emission model and the green curve shows the best fit powerlaw to  $T_B(\nu)$  with index  $\alpha_{mm}$ . Different markers show data from different observation cycles (denoted by ‘C’) and telescopes. (b):  $\alpha_{mm}$  versus  $T_{\text{eff}}$  for the ALMA detected stellar sample (Mohan et al., 2022). Bigger markers denoted old ( $>1$  Gyr) stars. Red line shows the power-law fit. A-type stars ( $T_{\text{eff}} > 8000$  K) are shown for comparison. (c):  $\alpha_{mm}$  versus pressure scale height for the same sample

have helped to identify weak flaring/star-planet interaction signatures in long-duration wideband monitoring data (e.g. Osten et al., 2008; Villadsen & Hallinan, 2019).

#### 4.1 Chromospheric tomography - a tool to characterise stellar activity

Based on the X-ray to optical and radio band observables, different stellar activity indicators have been constructed and studied as functions of physical parameters like stellar mass ( $M_*$ ),  $T_{\text{eff}}$ , age, rotation period ( $P_{\text{rot}}$ ), magnetic field strength etc. Common activity indicators include, the ratio of Ca-II H-K flux to bolometric flux ( $R'_{\text{HK}}$ , Noyes et al. (1984)) and the X-ray to bolometric flux ratio ( $R_X$ ). Though these indicators provide qualitative trends between activity and various physical parameters, a quantitative characterisation remains difficult due to the large variability in their values resulting from their complex dependencies on multiple parameters and physical processes (thermal, non-thermal and propagation effects) Stepien (1994); Pace (2013). This issue limits the insights that can be gained regarding the emergence of different levels and nature of activity from the atmospheres of different stellar types (Mohan et al., 2022).

##### 4.1.1 Exploring robust indicators of Chromospheric heating/activity

Observations and related models suggest that the atmospheric structure of cool stars significantly vary across spectral type or equivalently  $T_{\text{eff}}$  (e.g. Donati & Landstreet, 2009; Linsky, 2017). For the cool active stars it is known that the atmospheric heights extending from chromospheres to corona show signs of steady heating driven by their strong magnetic activity, which is also the driver of different space weather phenomena (Linsky, 2017; Vidotto et al., 2014). It is therefore highly desirable to construct a new and more reliable observational indicator of the quiescent atmospheric thermal structure of cool stars, which is closely linked to the atmospheric magnetic activity.

Recent solar and stellar observations demonstrated the unique tomographic potential of the  $mm$ -brightness spectrum to deduce the chromospheric thermal structure in cool stars

(Fig. 5a) (e.g. White et al., 2017b, 2020; Triglio et al., 2018; Mohan et al., 2021). Owing to their sensitivity down to  $\sim 20\mu\text{Jy}$  with a few hours integration, NOEMA and ALMA enable the detection of a sample of nearby stars in the mm band out to  $\sim 25\text{pc}$ . Using ALMA detected sample of cool stars, Mohan et al. (2022) showed that mm- $T_{\text{B}}(\nu)$  spectral indices ( $\alpha_{mm}$ ;  $T_{\text{B}}(\nu) \propto \nu^{-\alpha_{mm}}$ ) were positive for F – M dwarfs ( $T_{\text{eff}} \sim 7200 - 3000\text{K}$ ). Since lower frequencies probe higher heights, a positive  $\alpha_{mm}$  indicates progressively hotter and active outer atmospheres. The A-type stars with  $T_{\text{eff}} > 9000\text{K}$  showed negative  $\alpha_{mm}$  as expected from stars with no upper photospheric heating. The  $\alpha_{mm}$  versus  $T_{\text{eff}}$  showed an inverse trend suggesting that A6-9 type ( $T_{\text{eff}} \sim 7500 - 8000\text{K}$ ) stars could be the ones close to  $\alpha_{mm} \sim 0$ , marking the point of rise of chromospheric heating and activity in the main-sequence (Fig. 5b). Spectral line studies also suggest the same about late A-type stars (Simon et al., 2002; Linsky, 2017). Besides, Mohan et al. (2022) demonstrated that  $\alpha_{mm}$  can be a robust activity indicator since the power-law correlation functions between  $\alpha_{mm}$  and stellar physical parameters have much lower uncertainty ranges than those obtained with  $R'_{\text{HK}}$  and  $R_{\text{X}}$ . Also,  $\alpha_{mm}$  relates inversely to pressure scale heights in the atmosphere, as expected from a proxy to atmospheric thermal gradients (Fig. 5c).

## 5 Conclusions and outlook

The new generation sensitive, mm-radio interferometers are bringing about revolutionary changes in the exploration of solar/stellar activity. These instruments collectively provide extremely wideband data from 10 MHz to 1 THz at  $\lesssim \text{s}$  resolution. This snapshot spectroscopic data let us perform a tomographic exploration of solar/stellar atmospheres since different frequencies are sensitive to different heights in the atmosphere, ranging from upper photosphere to outer corona. The modern interferometers also employ a compact ‘large-N’ architecture which ensures dense u-v sampling leading to massive improvement in imaging fidelity and dynamic range for fine temporal ( $\lesssim 1\text{s}$ ) and spectral averaging ( $\sim 10\text{kHz}$  resolution in metrewave band;  $\sim 2\text{GHz}$  (continuum) and 0.01 - 10 MHz (spectral line) in mm band). This lets us do a continuous sampling of active atmospheric heights.

Modern instrumentation and data analysis tools/pipelines have lead to several novel discoveries and kick started new research avenues in solar/stellar activity in the recent years. However, much of these results and ventures are in an early phase, requiring more data and better models with detailed physics. There is hence a strong need to monitor the sun and stars, and gather more data during different periods of solar/stellar activity, varying in local physical conditions, energy levels and space weather impact. Analysing such datasets hold a lot of discovery potential to identify novel phenomena like the examples mentioned in the article, and also will help construct better physical models. Large volume of datasets is also an essential precursor to a detailed statistical characterisation/classification of the different types of active phenomena and exploring their space weather impacts/significance.

*Acknowledgements:* This work is supported by the Research Council of Norway through the EMISSA project (project number 286853) and the Centres of Excellence scheme, project number 262622 (“Rosseland Centre for Solar Physics”). This research made use of NASA’s Astrophysics Data System (ADS). AM is grateful to the developers of Python3

and various packages namely Numpy (Harris et al., 2020), Astropy (Astropy Collaboration et al., 2013), Scipy (Jones et al., 2001) and Matplotlib (Hunter, 2007).

## References

- Anantharamaiah K. R., Gothoskar P., Cornwell T. J., 1994, Radio Synthesis Imaging of Anisotropic Angular Broadening in the Solar Wind, *Journal of Astrophysics and Astronomy*, 15, 387
- Arzner K., Magun A., 1999, Radiowave propagation in a statistically inhomogeneous plasma, *A&A*, 351, 1165
- Aschwanden M. J., Freeland S. L., 2012, Automated Solar Flare Statistics in Soft X-Rays over 37 Years of GOES Observations: The Invariance of Self-organized Criticality during Three Solar Cycles, *ApJ*, 754, 112
- Astropy Collaboration et al., 2013, Astropy: A community Python package for astronomy, *A&A*, 558, A33
- Bain H. M., Krucker S., Saint-Hilaire P., Raftery C. L., 2014, Radio Imaging of a Type IVM Radio Burst on the 14th of August 2010, *ApJ*, 782, 43
- Barnes S. A., 2003, On the rotational evolution of solar- and late-type stars, its magnetic origins, and the possibility of stellar gyrochronology, *ApJ*, 586, 464
- Bastian T. S., Pick M., Kerdraon A., Maia D., Vourlidas A., 2001, The Coronal Mass Ejection of 1998 April 20: Direct Imaging at Radio Wavelengths, *ApJ*, 558, L65
- Callingham J. R., et al., 2021, The population of M dwarfs observed at low radio frequencies, *Nature Astronomy*, 5, 1233
- Callingham J. R., et al., 2022, V-LoTSS: The Circularly-Polarised LOFAR Two-metre Sky Survey, *arXiv e-prints*, p. *arXiv:2212.09815*
- Carley E. P., Vilmer N., Vourlidas A., 2020, Radio observations of coronal mass ejection initiation and development in the low solar corona, *Frontiers in Astronomy and Space Sciences*, 7, 79
- Chabrier G., Baraffe I., 2000, Theory of Low-Mass Stars and Substellar Objects, *ARA&A*, 38, 337
- Chen X., Kontar E. P., Chrysaphi N., Jeffrey N. L. S., Gordovskyy M., Yan Y., Tan B., 2020, Subsecond Time Evolution of Type III Solar Radio Burst Sources at Fundamental and Harmonic Frequencies, *ApJ*, 905, 43
- Chen B., et al., 2023, Radio Imaging Spectropolarimetry of CMEs and CME Progenitors, *arXiv e-prints*, p. *arXiv:2301.12188*
- Cliver E. W., Schrijver C. J., Shibata K., Usoskin I. G., 2022, Extreme solar events, *Living Reviews in Solar Physics*, 19, 2

- Coles W. A., Harmon J. K., Martin C. L., 1991, The solar wind density spectrum near the sun - Results from Voyager radio measurements, *J. Geophys. Res.*, *96*, 1745
- Crosley M. K., Osten R. A., 2018, Low-frequency Radio Transients on the Active M-dwarf EQ Peg and the Search for Coronal Mass Ejections, *ApJ*, *862*, 113
- Dal H., 2020, The flare cumulative frequencies of uv ceti stars from different spectral types, *MNRAS*, *495*, 4529
- Dennis B. R., 1985, Solar Hard X-Ray Bursts, *Sol. Phys.*, *100*, 465
- Donati J. F., Landstreet J. D., 2009, Magnetic Fields of Nondegenerate Stars, *ARA&A*, *47*, 333
- Eklund H., Wedemeyer S., Snow B., Jess D. B., Jafarzadeh S., Grant S. D. T., Carlsson M., Szydlarski M., 2021, Characterization of shock wave signatures at millimetre wavelengths from Bifrost simulations, *Philosophical Transactions of the Royal Society of London Series A*, *379*, 20200185
- Endo A., et al., 2010, A Catalog of Suzaku/WAM Hard X-Ray Solar Flares, *PASJ*, *62*, 1341
- Gary G. A., 2001, Plasma Beta above a Solar Active Region: Rethinking the Paradigm, *Sol. Phys.*, *203*, 71
- Gibson S., et al., 2016, FORWARD: A toolset for multiwavelength coronal magnetometry, *Frontiers in Astronomy and Space Sciences*, *3*, 8
- Güdel M., 2002, Stellar Radio Astronomy: Probing Stellar Atmospheres from Protostars to Giants, *ARA&A*, *40*, 217
- Guevara Gómez J. C., Jafarzadeh S., Wedemeyer S., Szydlarski M., Stangalini M., Fleck B., Keys P. H., 2021, High-frequency oscillations in small chromospheric bright features observed with Atacama Large Millimetre/Submillimetre Array, *Philosophical Transactions of the Royal Society of London Series A*, *379*, 20200184
- Harris C. R., et al., 2020, Array programming with NumPy, *Nature*, *585*, 357
- Henriques V. M. J., Jafarzadeh S., Guevara Gómez J. C., Eklund H., Wedemeyer S., Szydlarski M., Haugan S. V. H., Mohan A., 2022, The Solar ALMA Science Archive (SALSA). First release, SALAT, and FITS header standard, *A&A*, *659*, A31
- Hunter J. D., 2007, Matplotlib: A 2d graphics environment, *Computing in science & engineering*, *9*, 90
- Jafarzadeh S., et al., 2021, An overall view of temperature oscillations in the solar chromosphere with ALMA, *Philosophical Transactions of the Royal Society of London Series A*, *379*, 20200174

- Jeffrey N. L. S., Fletcher L., Labrosse N., 2017, Non-Gaussian Velocity Distributions in Solar Flares from Extreme Ultraviolet Lines: A Possible Diagnostic of Ion Acceleration, *ApJ*, 836, 35
- Jones E., Oliphant T., Peterson P., et al., 2001, SciPy: Open source scientific tools for Python, <http://www.scipy.org/>
- Kansabanik D., Mondal S., Oberoi D., 2023a, Deciphering Faint Gyrosynchrotron Emission from Coronal Mass Ejection using Spectro-polarimetric Radio Imaging, *arXiv e-prints*, p. *arXiv:2301.06522*
- Kansabanik D., Bera A., Oberoi D., Mondal S., 2023b, Tackling the Unique Challenges of Low-frequency Solar Polarimetry with the Square Kilometre Array Low Precursor: Pipeline Implementation, *ApJS*, 264, 47
- Klimchuk J. A., 2006, On Solving the Coronal Heating Problem, *Sol. Phys.*, 234, 41
- Klimchuk J. A., 2015, Key aspects of coronal heating, *Philosophical Transactions of the Royal Society of London Series A*, 373, 20140256
- Kontar E. P., et al., 2017a, Imaging spectroscopy of solar radio burst fine structures, *Nature Communications*, 8, 1515
- Kontar E. P., Perez J. E., Harra L. K., Kuznetsov A. A., Emslie A. G., Jeffrey N. L. S., Bian N. H., Dennis B. R., 2017b, Turbulent Kinetic Energy in the Energy Balance of a Solar Flare, *Phys. Rev. Lett.*, 118, 155101
- Kontar E. P., et al., 2019, Anisotropic Radio-wave Scattering and the Interpretation of Solar Radio Emission Observations, *ApJ*, 884, 122
- Kumari A., Ramesh R., Kathiravan C., Wang T. J., 2017a, Strength of the Solar Coronal Magnetic Field - A Comparison of Independent Estimates Using Contemporaneous Radio and White-Light Observations, *Sol. Phys.*, 292, 161
- Kumari A., Ramesh R., Kathiravan C., Gopalswamy N., 2017b, New Evidence for a Coronal Mass Ejection-driven High Frequency Type II Burst near the Sun, *ApJ*, 843, 10
- Leitzinger M., Odert P., Greimel R., Korhonen H., Guenther E. W., Hanslmeier A., Lammer H., Khodachenko M. L., 2014, A search for flares and mass ejections on young late-type stars in the open cluster Blanco-1, *Monthly Notices of the Royal Astronomical Society*, 443, 898
- Linsky J. L., 2017, Stellar model chromospheres and spectroscopic diagnostics, *Annual Review of Astronomy and Astrophysics*, 55, 159
- MacGregor M. A., Weinberger A. J., Wilner D. J., Kowalski A. F., Cranmer S. R., 2018, Detection of a Millimeter Flare from Proxima Centauri, *ApJ*, 855, L2
- Magara T., Shibata K., Yokoyama T., 1997, Evolution of Eruptive Flares. I. Plasmoid Dynamics in Eruptive Flares, *ApJ*, 487, 437

- Mahrous A., Alielden K., Vršnak B., Youssef M., 2018, Type II solar radio burst band-splitting: Measure of coronal magnetic field strength, *Journal of Atmospheric and Solar-Terrestrial Physics*, 172, 75
- Maia D. J. F., Gama R., Mercier C., Pick M., Kerdraon A., Karlický M., 2007, The Radio-Coronal Mass Ejection Event on 2001 April 15, *ApJ*, 660, 874
- Manoharan P. K., Ananthkrishnan S., 1990, Determination of solar-wind velocities using single-station measurements of interplanetary scintillation, *MNRAS*, 244, 691
- Mashonkina L., Sitnova T., Belyaev A. K., 2017, Influence of inelastic collisions with hydrogen atoms on the non-LTE modelling of Ca I and Ca II lines in late-type stars, *A&A*, 605, A53
- Masuda S., Kosugi T., Hara H., Tsuneta S., Ogawara Y., 1994, A loop-top hard X-ray source in a compact solar flare as evidence for magnetic reconnection, *Nature*, 371, 495
- McCauley P. I., Cairns I. H., Morgan J., 2018, Densities Probed by Coronal Type III Radio Burst Imaging, *Sol. Phys.*, 293, 132
- McCauley P. I., Cairns I. H., White S. M., Mondal S., Lenc E., Morgan J., Oberoi D., 2019, The Low-Frequency Solar Corona in Circular Polarization, *Sol. Phys.*, 294, 106
- McLean D., Labrum N., 1985, *Solar Radio Astrophysics*. Cambridge University Press
- McMullin J. P., Waters B., Schiebel D., Young W., Golap K., 2007, CASA Architecture and Applications, in *Astronomical Data Analysis Software and Systems XVI*, eds Shaw R. A., Hill F., Bell D. J., , *Astronomical Society of the Pacific Conference Series Vol. 376*, p. 127
- Mercier C., Trotter G., 1997, Coronal Radio Bursts: A Signature of Nanoflares?, *ApJ*, 474, L65
- Mohan A., 2021a, Characterising coronal turbulence using snapshot imaging of radio bursts in 80-200 MHz, *A&A*, 655, A77
- Mohan A., 2021b, Characterising coronal turbulence using snapshot imaging of radio bursts in 80-200 MHz, *A&A*, 655, A77
- Mohan A., 2021c, Discovery of Correlated Evolution in Solar Noise Storm Source Parameters: Insights on Magnetic Field Dynamics during a Microflare, *ApJ*, 909, L1
- Mohan A., Oberoi D., 2017, 4D Data Cubes from Radio-Interferometric Spectroscopic Snapshot Imaging, *Sol. Phys.*, 292, 168
- Mohan A., Mondal S., Oberoi D., Lonsdale C. J., 2019a, Evidence for super-alfvénic oscillations in solar type III radio burst sources, *ApJ*, 875, 98
- Mohan A., McCauley P. I., Oberoi D., Mastrano A., 2019b, A Weak Coronal Heating Event Associated with Periodic Particle Acceleration Episodes, *ApJ*, 883, 45



- Mohan A., Wedemeyer S., Pandit S., Saberi M., Hauschildt P. H., 2021, EMISSA (Exploring Millimeter Indicators of Solar-Stellar Activity). I. The initial millimeter-centimeter main-sequence star sample, *A&A*, 655, A113
- Mohan A., Wedemeyer S., Hauschildt P. H., Pandit S., Saberi M., 2022, EMISSA (Exploring millimetre indicators of solar-stellar activity). II. Towards a robust indicator of stellar activity, *A&A*, 664, L9
- Mondal S., 2021, A Search for the Counterparts of Quiet-Sun Radio Transients in Extreme Ultraviolet Data, *Sol. Phys.*, 296, 131
- Mondal S., Mohan A., Oberoi D., Morgan J. S., Benkevitch L., Lonsdale C. J., Crowley M., Cairns I. H., 2019, Unsupervised generation of high dynamic range solar images: A novel algorithm for self-calibration of interferometry data, *ApJ*, 875, 97
- Mondal S., Oberoi D., Vourlidis A., 2020, Estimation of the Physical Parameters of a CME at High Coronal Heights Using Low-frequency Radio Observations, *ApJ*, 893, 28
- Morosan D. E., et al., 2014, LOFAR tied-array imaging of Type III solar radio bursts, *A&A*, 568, A67
- Morosan D. E., et al., 2019, Multiple regions of shock-accelerated particles during a solar coronal mass ejection, *Nature Astronomy*, 3, 452
- Morosan D. E., Pomoell J., Kumari A., Vainio R., Kilpua E. K. J., 2022, Shock-accelerated electrons during the fast expansion of a coronal mass ejection, *A&A*, 668, A15
- Mugundhan V., Hariharan K., Ramesh R., 2017, Solar Type IIIb Radio Bursts as Tracers for Electron Density Fluctuations in the Corona, *Sol. Phys.*, 292, 155
- Mullan D. J., Paudel R. R., 2019, Origin of radio-quiet coronal mass ejections in flare stars, *ApJ*, 873, 1
- Namekata K., et al., 2017, Statistical Studies of Solar White-light Flares and Comparisons with Superflares on Solar-type Stars, *ApJ*, 851, 91
- Namekata K., et al., 2022, Discovery of a Long-duration Superflare on a Young Solar-type Star EK Draconis with Nearly Similar Time Evolution for H $\alpha$  and White-light Emissions, *ApJ*, 926, L5
- Narang N., Chandrashekhar K., Jafarzadeh S., Fleck B., Szydlarski M., Wedemeyer S., 2022, Power distribution of oscillations in the atmosphere of a plage region. Joint observations with ALMA, IRIS, and SDO, *A&A*, 661, A95
- Nelson G. J., Melrose D. B., 1985, in eds McLean D. J., Labrum N. R., , , Solar Radiophysics: Studies of Emission from the Sun at Metre Wavelengths. pp 333–359
- Nindos A., Patsourakos S., Jafarzadeh S., Shimojo M., 2022, The dynamic chromosphere at millimeter wavelengths, *Frontiers in Astronomy and Space Sciences*, 9, 981205

- Noyes R. W., Hartmann L. W., Baliunas S. L., Duncan D. K., Vaughan A. H., 1984, Rotation, convection, and magnetic activity in lower main-sequence stars., *ApJ*, 279, 763
- Oberoi D., et al., 2011, First Spectroscopic Imaging Observations of the Sun at Low Radio Frequencies with the Murchison Widefield Array Prototype, *ApJ*, 728, L27
- Oberoi D., Bisoi S. K., Sasikumar Raja K., Kansabanik D., Mohan A., Mondal S., Sharma R., 2022, Preparing for Solar and Heliospheric Science with the SKAO: An Indian Perspective, *arXiv e-prints*, p. arXiv:2211.03791
- Odert P., Leitzinger M., Guenther E. W., Heinzel P., 2020, Stellar coronal mass ejections - II. Constraints from spectroscopic observations, *MNRAS*, 494, 3766
- Offringa A. R., 2010, AOFlogger: RFI Software, Astrophysics Source Code Library, record ascl:1010.017 (ascl:1010.017)
- Osten R. A., Hawley S. L., Allred J. C., Johns-Krull C. M., Roark C., 2005, From Radio to X-Ray: Flares on the dMe Flare Star EV Lacertae, *ApJ*, 621, 398
- Osten R. A., et al., 2008, Ultrahigh Time Resolution Observations of Radio Bursts on AD Leonis, *ApJ*, 674, 1078
- Pace G., 2013, Chromospheric activity as age indicator. An L-shaped chromospheric-activity versus age diagram, *A&A*, 551, L8
- Parker E. N., 1963, The Solar-Flare Phenomenon and the Theory of Reconnection and Annihilation of Magnetic Fields., *ApJS*, 8, 177
- Pauluhn A., Solanki S. K., 2007, A nanoflare model of quiet Sun EUV emission, *A&A*, 462, 311
- Rahman M. M., McCauley P. I., Cairns I. H., 2019, On the Relative Brightness of Coronal Holes at Low Frequencies, *Sol. Phys.*, 294, 7
- Ramesh R., Kathiravan C., 2022, Polarization Observations of a Split-band Type II Radio Burst from the Solar Corona, *ApJ*, 940, 80
- Ramesh R., Sasikumar Raja K., Kathiravan C., Narayanan A. S., 2013, Low-frequency Radio Observations of Picoflare Category Energy Releases in the Solar Atmosphere, *ApJ*, 762, 89
- Reid H. A. S., Kontar E. P., 2021, Fine structure of type III solar radio bursts from Langmuir wave motion in turbulent plasma, *Nature Astronomy*, 5, 796
- Reid H. A. S., Ratcliffe H., 2014, A review of solar type III radio bursts, *Research in Astronomy and Astrophysics*, 14, 773
- Robinson R. D., 1983, Scattering of radio waves in the solar corona, *Proceedings of the Astronomical Society of Australia*, 5, 208

- Saint-Hilaire P., Vilmer N., Kerdraon A., 2013, A Decade of Solar Type III Radio Bursts Observed by the Nançay Radioheliograph 1998-2008, *ApJ*, 762, 60
- Sasikumar Raja K., Ramesh R., Hariharan K., Kathiravan C., Wang T. J., 2014, An Estimate of the Magnetic Field Strength Associated with a Solar Coronal Mass Ejection from Low Frequency Radio Observations, *ApJ*, 796, 56
- Sasikumar Raja K., Subramanian P., Ramesh R., Vourlidis A., Ingale M., 2017, Turbulent Density Fluctuations and Proton Heating Rate in the Solar Wind from 9-20 R<sub>☉</sub>, *ApJ*, 850, 129
- Segura A., Walkowicz L. M., Meadows V., Kasting J., Hawley S., 2010, The Effect of a Strong Stellar Flare on the Atmospheric Chemistry of an Earth-like Planet Orbiting an M Dwarf, *Astrobiology*, 10, 751
- Sharma R., Oberoi D., 2020, Propagation Effects in Quiet Sun Observations at Meter Wavelengths, *ApJ*, 903, 126
- Sharma R., Oberoi D., Arjunwadkar M., 2018, Quantifying Weak Nonthermal Solar Radio Emission at Low Radio Frequencies, *ApJ*, 852, 69
- Sharma R., Oberoi D., Battaglia M., Krucker S., 2022, Detection of Ubiquitous Weak and Impulsive Nonthermal Emissions from the Solar Corona, *ApJ*, 937, 99
- Sharykin I. N., Kontar E. P., Kuznetsov A. A., 2018, LOFAR Observations of Fine Spectral Structure Dynamics in Type IIIb Radio Bursts, *Sol. Phys.*, 293, 115
- Shibata K., et al., 2007, Chromospheric Anemone Jets as Evidence of Ubiquitous Reconnection, *Science*, 318, 1591
- Simon T., Ayres T. R., Redfield S., Linsky J. L., 2002, Limits on Chromospheres and Convection among the Main-Sequence A Stars, *ApJ*, 579, 800
- Skumanich A., 1972, Time Scales for Ca II Emission Decay, Rotational Braking, and Lithium Depletion, *ApJ*, 171, 565
- Steinberg J. L., Aubier-Giraud M., Leblanc Y., Boischot A., 1971, Coronal Scattering, Absorption and Refraction of Solar Radiobursts, *A&A*, 10, 362
- Stepien K., 1994, Applicability of the Rossby number in activity-rotation relations for dwarfs and giants., *A&A*, 292, 191
- Suresh A., et al., 2017, Wavelet-based Characterization of Small-scale Solar Emission Features at Low Radio Frequencies, *ApJ*, 843, 19
- Testa P., et al., 2013, Observing Coronal Nanoflares in Active Region Moss, *ApJ*, 770, L1
- Testa P., et al., 2014, Evidence of nonthermal particles in coronal loops heated impulsively by nanoflares, *Science*, 346, 1255724

- Thejappa G., MacDowall R. J., 1998, Evidence for Strong and Weak Turbulence Processes in the Source Region of a Local Type III Radio Burst, *ApJ*, 498, 465
- Thejappa G., Macdowall R. J., 2018, Langmuir solitons in solar type iii radio bursts: Stereo observations, *The Astrophysical Journal*, 864
- Trigilio C., et al., 2018, Detection of  $\alpha$  Centauri at radio wavelengths: chromospheric emission and search for star-planet interaction, *MNRAS*, 481, 217
- Vedantham H. K., 2020, Prospects for radio detection of stellar plasma beams, *A&A*, 639, L7
- Vedantham H. K., 2021, On the mechanism of polarized metre-wave stellar emission, *MNRAS*, 500, 3898
- Vedantham H. K., et al., 2020, Coherent radio emission from a quiescent red dwarf indicative of star-planet interaction, *Nature Astronomy*, 4, 577
- Vedantham H. K., Callingham J. R., Shimwell T. W., Benz A. O., Hajduk M., Ray T. P., Tasse C., Drabent A., 2022, Peculiar Radio-X-Ray Relationship in Active Stars, *ApJ*, 926, L30
- Viall N. M., Klimchuk J. A., 2017, A Survey of Nanoflare Properties in Active Regions Observed with the Solar Dynamics Observatory, *ApJ*, 842, 108
- Vidotto A. A., et al., 2013, Effects of M dwarf magnetic fields on potentially habitable planets, *A&A*, 557, A67
- Vidotto A. A., et al., 2014, Stellar magnetism: empirical trends with age and rotation, *MNRAS*, 441, 2361
- Villadsen J., Hallinan G., 2019, Ultra-wideband Detection of 22 Coherent Radio Bursts on M Dwarfs, *ApJ*, 871, 214
- Wedemeyer S., et al., 2016, Solar Science with the Atacama Large Millimeter/Submillimeter Array—A New View of Our Sun, *Space Sci. Rev.*, 200, 1
- White S. M., 2004, The solar stellar connection, *New A Rev.*, 48, 1319
- White S., 2007, Solar radio bursts and space weather, *Asian J. Phys.*, 16, 189
- White S. M., et al., 2017a, Observing the Sun with the Atacama Large Millimeter/submillimeter Array (ALMA): Fast-Scan Single-Dish Mapping, *Sol. Phys.*, 292, 88
- White S. M., et al., 2017b, Observing the Sun with the Atacama Large Millimeter/submillimeter Array (ALMA): Fast-Scan Single-Dish Mapping, *Sol. Phys.*, 292, 88
- White J. A., et al., 2020, The MESAS Project: ALMA Observations of the F-type Stars  $\gamma$  Lep,  $\gamma$  Vir A, and  $\gamma$  Vir B, *ApJ*, 894, 76

- Wild J. P., 1970, Some Investigations of the Solar Corona: The First Two Years of Observation With the Culgoora Radioheliograph, *Proceedings of the Astronomical Society of Australia*, 1, 365
- Yashiro S., Gopalswamy N., Michalek G., St. Cyr O. C., Plunkett S. P., Rich N. B., Howard R. A., 2004, A catalog of white light coronal mass ejections observed by the SOHO spacecraft, *Journal of Geophysical Research (Space Physics)*, 109, A07105
- Zhang P., et al., 2022, Imaging of the Quiet Sun in the Frequency Range of 20-80 MHz, *ApJ*, 932, 17
- Zhang P., Offringa A. R., Zucca P., Kozarev K., Mancini M., 2023, RFI Flagging in Solar and Space Weather Low Frequency Radio Observations, *MNRAS*,
- Zhou Y.-A., Hong J., Li Y., Ding M. D., 2022, Diagnosing the Optically Thick/Thin Features Using the Intensity Ratio of Si IV Resonance Lines in Solar Flares, *ApJ*, 926, 223
- Zic A., et al., 2020, A Flare-type IV Burst Event from Proxima Centauri and Implications for Space Weather, *ApJ*, 905, 23
- Zucca P., Carley E. P., Bloomfield D. S., Gallagher P. T., 2014, The formation heights of coronal shocks from 2D density and Alfvén speed maps, *A&A*, 564, A47
- Zucca P., et al., 2018, Shock location and CME 3D reconstruction of a solar type II radio burst with LOFAR, *A&A*, 615, A89